

This document is the Accepted Manuscript version of a Published Work that appeared in final form in ACS Biomaterials Science & Engineering, copyright © American Chemical Society after peer review and technical editing by the publisher. To access the final edited and published work see <https://doi.org/10.1021/acsbiomaterials.2c00034>.

Access to this work was provided by the University of Maryland, Baltimore County (UMBC) ScholarWorks@UMBC digital repository on the Maryland Shared Open Access (MD-SOAR) platform.

Please provide feedback

Please support the ScholarWorks@UMBC repository by emailing scholarworks-group@umbc.edu and telling us what having access to this work means to you and why it's important to you. Thank you.



Published in final edited form as:

ACS Biomater Sci Eng. 2022 June 13; 8(6): 2574–2588. doi:10.1021/acsbiomaterials.2c00034.

Peripheral Nerve Decellularization for *In Vitro* Extracellular Matrix Hydrogel Use: A Comparative Study

Emory Gregory,

Department of Biomedical Engineering, University of Arkansas, Fayetteville, Arkansas 72701, United States

In Ha Baek,

Department of Biomedical Engineering, University of Arkansas, Fayetteville, Arkansas 72701, United States

Nikolas Ala-Kokko,

Department of Biomedical Engineering, University of Arkansas, Fayetteville, Arkansas 72701, United States

Reagan Dugan,

Department of Biomedical Engineering, University of Arkansas, Fayetteville, Arkansas 72701, United States

Luis Pinzon-Herrera,

Ralph E. Martin Department of Chemical Engineering, University of Arkansas, Fayetteville, Arkansas 72701, United States

Jorge Almodóvar,

Ralph E. Martin Department of Chemical Engineering, University of Arkansas, Fayetteville, Arkansas 72701, United States

Young Hye Song

Department of Biomedical Engineering, University of Arkansas, Fayetteville, Arkansas 72701, United States

Abstract

The rise of tissue-engineered biomaterials has introduced more clinically translatable models of disease, including three-dimensional (3D) decellularized extracellular matrix (dECM) hydrogels. Specifically, decellularized nerve hydrogels have been utilized to model peripheral nerve injuries and disorders *in vitro*; however, there lacks standardization in decellularization methods. Here, rat sciatic nerves of varying preparations were decellularized using previously established methods:

Corresponding Author: Young Hye Song – *Department of Biomedical Engineering, University of Arkansas, Fayetteville, Arkansas 72701, United States*; Phone: 479-575-5008; yhsong@uark.edu.

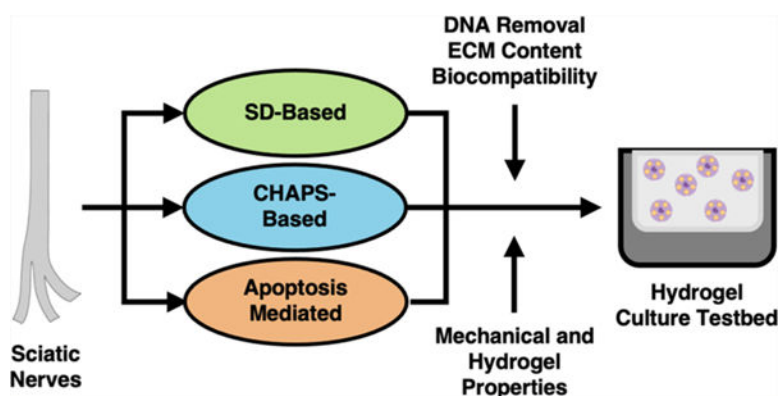
Author Contributions

E.G. and Y.H.S. conceived the study design. E.G. was responsible for experimentations and data analyses, unless noted otherwise. I.H.B. performed rheological characterization and aided in Luminex analysis. N.A.-K. performed confocal reflectance imaging of the dECM hydrogels. R.D. aided decellularization, DNA isolation, and immunohistochemistry. L.P.-H. and J.A. assisted in Luminex training and performance. E.G. and Y.H.S. interpreted data and wrote the manuscript. All co-authors were involved in the final editing of the manuscript.

The authors declare no competing financial interest.

sodium deoxycholate (SD)-based, 3-((3-cholamidopropyl)-dimethylammonio)-1-propanesulfonate (CHAPS)-based, and apoptosis-mediated. These nerves were characterized for cellular debris removal, ECM retention, and low cytotoxicity with cultured Schwann cells. The best preparations of each decellularization method were digested into dECM hydrogels, and rheological characterization, gelation kinetics, and confocal reflectance imaging of collagen fibril assembly were performed. It was determined that the SD-based method with nerve epineurial removal best maintained the overall ECM composition and mechanical properties of physiological peripheral nerves while efficiently stripping the scaffolds of tissue-specific cells and debris. This method was then utilized as a culture platform for quiescent Schwann cells and cancer–nerve crosstalk. Hydrogel-embedded Schwann cells were found to have high viability and act in a more physiologically relevant manner than those cultured in monolayers, and the hydrogel platform allowed for the activation of Schwann cells following treatment with cancer secreted factors. These findings establish a standard for peripheral nerve decellularization for usage as a dECM hydrogel testbed for *in vitro* peripheral nerve disease modeling and may facilitate the development of treatments for peripheral nerve disease and injury.

Graphical Abstract



Keywords

sciatic nerves; decellularized extracellular matrix; mechanical and hydrogel properties; peripheral nerve disease

1. INTRODUCTION

The natural extracellular matrix (ECM) is the noncellular network composed of a multitude of macromolecules, including glycoproteins, proteoglycans, and glycosaminoglycans (GAGs), that provides the biochemical and biomechanical cues necessary for cell survival.^{1–4} As a particularly abundant component of the ECM, collagen provides structural integrity by producing triple-stranded helices that establish fibrils to construct the interstitial tissue stroma (e.g., collagens I, II, III) and basal membrane (e.g., collagen IV).⁵ Along with collagen, ECM components including fibronectin, proteoglycans, and GAGs (e.g., chondroitin sulfate and heparan sulfate proteoglycans) mediate cell attachment and function by binding molecular components to tissue scaffolds while laminin aids in basement

membrane formation to modulate tissue morphology.^{4,6,7} The ECM is highly dynamic and differs between tissue types based on the ratio of compositional macromolecules.⁸

In healthy tissue, the ECM regularly undergoes remodeling, but the onset of injury or disease can lead to a dysregulation of tissue homeostasis.^{9,10} During this disturbance, specialized enzymes are upregulated to digest fibrillar collagens, laminin, fibronectin, and other ECM components, altering the tissue microenvironment and potentially phenotype of embedded cells.^{11,12} Traditional two-dimensional (2D) *in vitro* cell culture techniques fail to incorporate the three-dimensional (3D) ECM, so these models of disease lack the inclusion of any disruption in cellular mechanism that may normally occur in the native microenvironment. For this reason, 2D cell studies have been criticized for insufficiently producing physiologically relevant results.^{12–17} As a result, *in vivo* animal studies were previously seen as more reliable; however, these models have been found to have low reproducibility, high cost, and lack clinical translatability.^{18,19} Therefore, the relatively new field of tissue engineering has become increasingly popular for creating models that generate physiologic systems of the ECM and disease.^{20–23}

Within the past two decades, decellularization of animal tissue has been utilized to fabricate natural acellular biomaterials that may be implemented in *in vitro* studies to create physiologically relevant disease mimics.^{22,24–26} This process involves the removal of specialized cells from tissues or organs through enzymatic intervention, physical distress, and/or chemical treatment.^{27,28} This removal of cells is important for both disease modeling and regenerative medicine applications, as a clean scaffold is needed to ensure proper cellular composition and biomolecular and biomechanical properties of the designed model as well as the absence of response by embedded immune cells.^{3,29,30} Enzymatic decellularization utilizes nucleases and/or proteinases to remove cellular components, while freeze–thaw cycles, high hydrostatic pressure, mechanical agitation, and/or supercritical CO₂ are applied during physical decellularization to reduce the risk of cytotoxicity by residual reagents.^{31–33} Chemical decellularization is particularly prevalent in tissue engineering; these processes involve washes of hypo/hypertonic salt solutions, acids, bases, solvents, and/or detergents to produce clean tissue scaffolds.³⁴ Detergents, in particular, are prominent reagents utilized in published decellularization methods.³⁵

Ionic detergents, such as sodium deoxycholate (SD), denature proteins and disrupt cell–nucleic membrane connections to remove genetic material, while nonionic detergents, such as Triton X-100, deactivate small chains of amino acids and interrupt DNA–protein, lipid–lipid, and lipid–protein connections.^{36,37} Zwitterionic detergents, such as sulfobetaine-10 (SB-10), SB-16, and CHAPS, share qualities from both ionic and nonionic detergents; these chemicals maintain the structural integrity of the ECM but can contribute to increased protein deactivation compared to other detergent types. Additionally, hypo/hypertonic solutions remove cells via swelling and lysis without the risk of ECM compromise.³⁸ As both chemical and physical decellularizations generally involve the necrosis of cellular components, the methods are often used in conjunction to efficiently clean ECM scaffolds of necrotic cell debris; however, this increases the risk for excess ECM damage. As an alternative, methods have been optimized to implement cell apoptosis, rather than necrosis, to avoid excess chemical usage; these methods have shown success in ECM retention.^{35,39}

Hydrogels are versatile biomaterials applicable to both *in vitro* and *in vivo* studies and are considered beneficial for their high permeability, cell viability, and tunable mechanical characteristics.^{30,40–44} While natural and synthetic polymers are commonly used to create hydrogels, decellularized natural ECM (dECM) hydrogels are advantageous in replicating native tissue milieu. Decellularized tissues with a significant reduction in cell and genetic debris can easily be homogenized and digested with an acid/enzyme solution to produce hydrogels.⁴⁵ These gels have historically been valued for their *in vivo* tissue regeneration applications due to their biocompatible properties, but they are becoming increasingly popular as *in vitro* 3D platforms for disease modeling.^{21,46,47} Studies employing these dECM hydrogels uniquely provide more relevant models of clinical cell phenotype compared to traditional 2D cell culture and studies.^{48,49}

In this study, we investigated three peripheral nerve decellularization protocols and measured success via neural cell and DNA removal, ECM retention, and absence of cytotoxicity.^{33,50,51} Additionally, within each method, murine sciatic nerves were prepared in three different ways to determine the relationship between reagent penetration and successful decellularization: epineurial removal, transverse dissection, and epineurial removal following dissection. Immunohistochemistry (IHC), DNA isolation, and cell metabolism assays were performed to evaluate the validity of each method. Following optimization, nerves with the top preparations of each decellularization method were digested into dECM hydrogels and evaluated for collagen fibril assembly and mechanical properties. The overall best method was established and was utilized as dECM hydrogels for 3D Schwann cell culture platforms. Cytokine secretion of 3D-cultured cells was analyzed and compared against that of 2D-cultured Schwann cells, and embedded Schwann cells were treated with cancer secreted factors to verify the testbed's ability to model disease. Here, we found that nerves prepared via SD-based decellularization with epineurial removal have the best cell removal and ECM retention overall, and its resulting dECM hydrogel showed evidence of a dense fibrillar collagen network formation and biomimetic mechanical properties. When used as a Schwann cell culture platform, 3D-cultured cells presenting with phenotypes more similar to that *in vivo* versus those cultured in 2D, and embedded Schwann cells exhibited a shift in activated phenotype when cultured with cancer secreted factors. We propose this protocol to be implemented as a standard for *in vitro* modeling of peripheral nerve diseases, injuries, and disorders, especially because a majority of the currently established peripheral nerve decellularization protocols are equipped for usage in *in vivo* regenerative medicine scenarios.^{52–57} The use of this hydrogel could create a more physiologically relevant model of the disease and can potentially provide more clinically translatable results compared to traditional 2D studies.

2. EXPERIMENTAL SECTION

2.1. Chemicals and Antibodies.

The following chemicals were purchased from VWR: phosphate-buffered saline (PBS; 97062–948), sodium chloride (BDH9286), sodium dihydrogen phosphate monohydrate (BDH9298), disodium hydrogen phosphate heptahydrate (BDH9296), magnesium chloride hexahydrate (BDH9244), 200 proof pure ethanol (89125–188), xylene (MK866816),

and Fluoromount G (100241–874). Dulbecco's Modified Eagle's Medium (DMEM; 30–2002) was purchased from ATCC. Sylgard 184 Silicone Elastomer Kit (01317318) was purchased from DOW Chemical Company. The following chemicals were purchased from Sigma-Aldrich: SB-10 (D4266), SD (D6750), SB-16 (H6883), deoxyribonuclease I (D4527), chondroitinase ABC (ChABC; C3667), CHAPS (220201), aprotinin (A1153), ribonuclease A (R4875), trizma hydrochloride (T3253), formaldehyde solution (252549), hematoxylin solution, Harris modified (HHS32), eosin Y solution (HT110216), DPX mountant (06522), trichrome stain (Masson) kit (HT15), Triton X-100 BioUltra (93443), goat serum (69023), pepsin (P7000), alcian blue (66011), hydrochloric acid (320331), sodium hydroxide (415413), medium 199 (M0650), poly-(ethyleneimine) (PEI; 181978), glutaraldehyde (GA; G6257), forskolin from *Coleus forskohlii* (F6886), Tween-20 (P9416), poly-L-lysine (P4707), and glycine (410225). The following chemicals were purchased from Thermo Fisher: camptothecin (ICN15973283), alamarBlue Cell Viability Reagent (DAL1100), penicillin–streptomycin (P/S; 15140163), and Live/Dead Cell Imaging Kit (R37601). QuantiFluor dsDNA System (2670) was purchased from Promega, and fetal bovine serum (FBS; S11150) and Human Luminex Discovery Assay (LXSAHM-03) were purchased from R&D Systems.

The following antibodies were purchased from Thermo Fisher: mouse anti-S100 (1:400; MA126621), rabbit anti- β -III tubulin (1:1000; PA5–85639), mouse anti-collagen I (1:2000; MA1–26771), mouse anti-fibronectin (1:250; MA5–11981), and rabbit anti-laminin (1:1000; PA1–16730), DAPI (1:2500; D1206), goat anti-mouse Alexa Fluor 568 (1:500; A11031), and goat anti-rabbit Alexa Fluor 647 (1:500; A21244). Abcam was used to purchase the following: rabbit anti-collagen IV (1:500; ab6586), mouse anti-chondroitin sulfate (CSPG; 1:400; ab11570), rabbit anti-heparan sulfate (HSPG; 1:400; ab2501), rabbit anti-glial fibrillary acidic protein (GFAP; 1:100; ab16997), and rabbit anti-Ki67 (1:200; ab16667).

2.2. Tissue Acquisition.

All animal work was approved by the Institutional Animal Care and Use Committee (IACUC) of the University of Arkansas. Adult male Sprague Dawley rats (7–12 weeks) weighing 300–400 g were purchased from Charles River and Envigo and cared for by the staff of the Central Laboratory Animal Facility (CLAF) in accordance with the IACUC Standards and the Animal Welfare Act. Rats had access to 12 h light/dark cycles and standard food and water *ad libitum*. Rats were euthanized in ordinance with the American Veterinary Medical Association guidelines via carbon dioxide asphyxiation. Rats were also donated by Dr. Jeffrey Wolchok in the Department of Biomedical Engineering at the University of Arkansas, Fayetteville, AR.

Sciatic nerves harvest was performed aseptically. Nerves were prepared by removing the epineurium, which was established as preparation A; dissecting in half (preparation B) or dissection upon epineurial removal (preparation C). Nerves were frozen at -20°C in $1\times$ phosphate-buffered saline (PBS) or for immediate use placed on ice in basal DMEM based on the assigned decellularization method.

2.3. Decellularization.

Rat sciatic nerves were prepared and then decellularized using one of three previously established methods (Figure 1A).^{33,50,51} Decellularization groups are identified in Figure 1B. Decellularization was performed at room temperature with 14 rpm agitation in 15 mL of solution unless otherwise stated.

2.3.1. Method 1 (SD-Based).—Nerves were thawed and rinsed in deionized water (dH₂O) for 7 h.³³ Nerves were washed in 125 mM SB-10 in 50 mM sodium/10 mM phosphate buffer (buffer 1) for 18 h and rinsed in 100 mM sodium/50 mM phosphate buffer (buffer 2) for 15 min (Figure 1C). Nerves were washed in 3% SD (w/v) and 0.6 mM SB-16 in buffer 1 for 2 h and rinsed three times for 15 min in buffer 2. Nerves were washed SB-10 in buffer 1 for 7 h once again and rinsed for 15 min in buffer 2. Nerves were again washed SD/SB-16 in buffer 1 for 1.5 h and rinsed for 15 min three times in buffer 1. Nerves were treated statically in 1 mL of 75 U/mL DNase in buffer 1 for 3 h and rinsed three times in buffer 1 for 1 h cycles. Nerves were incubated statically in 0.2 mL of 0.2 U/mL ChABC in PBS for 16 h at 37 °C. Nerves were finally rinsed in PBS for 9 h cycles, with reagent changes every 3 h, and then frozen at –20 °C overnight or prepared for histology.

2.3.2. Method 2 (CHAPS-Based).—Nerves were thawed and washed in dH₂O for 7 h.⁵⁰ Nerves were washed in 100 mM CHAPS/10 KIU/mL aprotinin in PBS for 24 h and rinsed in 1 M sodium chloride for 15 h (Figure 1D). Nerves were statically incubated in 1 mL of 10 µg/mL DNase/200 µg/mL RNase/10 mM Tris-hydrochloride solution for 24 h at 37 °C. Nerves were rinsed in PBS for 72 h and frozen at –20 °C overnight or prepared for histology.

2.3.3. Method 3 (Apoptosis-Mediated).—Freshly harvested nerves were placed in basal DMEM until all nerves were harvested.⁵¹ The nerves were washed in 5 µM camptothecin in DMEM for 24 h at 37 °C (Figure 1E). The nerves were then washed in 4× PBS for 24 h, 2× PBS for 30 min, and three times in 1× PBS for 30 min. The nerves were incubated without agitation in 1 mL of 75 U/mL DNase in PBS for 36 h. The nerves were rinsed in PBS twice in 30 min increments and frozen at –20 °C overnight or prepared for histology.

2.4. DNA Isolation and Analysis.

Fresh and decellularized nerves were lyophilized using the Labconco FreeZone 4.5 lyophilizer for 3 days and then weighed in mg (W). DNA was isolated from nerves using a modified protocol by Qiagen. Eluted DNA volume in µL was recorded (V). DNA was combined with QuantiFluor dsDNA System dye, and fluorescence was measured using a plate reader (BioTek Synergy Mix Microplate Reader) at 504 nm excitation/531 nm emission. Measured DNA concentration in ng/µL was computed (C_M) by comparing to a dsDNA standard. The actual of ng dsDNA per mg of dry nerve tissue (C_A) was calculated using eq 1

$$C_A = \frac{C_M \times V}{W} \quad (1)$$

2.5. Tissue Cytotoxicity.

Thawed fresh and decellularized nerves were added to DMEM with 1% P/S in triplicate into 24-well plates and incubated at 37 °C for 3 days. After incubation, 10% (v/v) FBS was added to the eluted media and used to culture passage 4 of human sNF96.2 Schwann-like cells (ATCC; CRL-2884) with a density of 500k cells per well. Cells were cultured for 2 days. AlamarBlue was combined with DMEM with 10% FBS/1% P/S (complete media) 1:9 and added to the cells. Cells were incubated for 3 h. The absorbances of sample-conditioned media (A_S) were measured at 570 nm excitation/600 nm emission to assess the percent reduction from resazurin to resorufin, which correlates to cell metabolism, and evaluated against cells cultured with complete media only (A_0). Percent reduction of metabolic activity was computed using eq 2

$$\% \text{ reduction} = \frac{A_0 - A_S}{A_0} \times 100\% \quad (2)$$

2.6. Tissue Immunohistochemistry.

All preparation steps were performed at 4 °C. Nerves were fixed with 3.7% formaldehyde in PBS overnight. The nerves were preserved by treatments in 10 and 30% sucrose for 1 and 6 days, respectively, and then allowed to soak in optimal cutting temperature reagent (OCT) with high humidity before frozen at –80 °C overnight. The nerves were sectioned at 10–11 μm using a cryotome (Leica), dried at room temperature overnight, and stored at –80 °C. Before staining, all samples were thawed at 40 °C for 30 min. All samples were imaged using the Olympus IX83 inverted microscope.

2.6.1. Hematoxylin and Eosin (H&E).—Samples were stained in Harris hematoxylin and eosin Y and finished with ethanol and xylene dehydration steps. Slides were mounted with DPX mounting medium and allowed to dry overnight at room temperature.

2.6.2. Masson's Trichrome (Trichrome).—Trichrome was performed using the protocol provided by the Trichrome stain (Masson) kit. Samples were dehydrated in ethanol and xylene, mounted with DPX mounting medium, and allowed to dry overnight at room temperature.

2.6.3. Alcian Blue.—Samples were incubated in alcian blue for 5 min at room temperature, immediately followed by a 15 min rinse in running water. Slides were dried with 100% ethanol and xylene and were mounted with DPX mounting medium and allowed to dry overnight at room temperature.

2.6.4. Immunohistochemistry (IHC).—Tissue samples were washed in a 3:3:94 (v/v) 3% goat serum/0.3% Triton X-100/PBS blocking buffer 1 h at room temperature and incubated for 24 h with primary antibodies at 4 °C. The slides were rinsed with PBS three times in 10 min intervals and then incubated in secondary antibodies away from light at 4 °C for 24 h. The samples were rinsed in PBS three times for 10 min and incubated with DAPI away from light for 5 min. Slides were rinsed in PBS and mounted with Fluoromount G. Slides were sealed with clear nail polish and allowed to dry overnight.

2.7. Photolithography.

Soft lithography was utilized to produce poly(dimethylsiloxane) (PDMS) microwells for 3D culture.⁵⁸ Briefly, a clean silicon wafer was coated with SU-8 photoresist and arrays of cylindrical patterns of 4 mm in diameter and 200 μm in depth were created. Silicone elastomer base and curing agent were mixed well at a 10:1 ratio, air bubbles removed, added to the wafer, and cured at 60 °C for 2 h. The resulting microwells and smooth PDMS lids were biopsy-punched and prepared for 3D culture.

2.8. Hydrogel Digestion and Characterization.

Decellularized nerves were lyophilized for 2–3 days. Nerves were weighed, minced, and added to a 20 mL tube with a stir bar before being digested at 12 mg/mL in a 1 mg/mL pepsin and 0.01 M hydrochloric acid solution. The tube was placed on a stir plate at 400–500 rpm for 2–3 days at room temperature.

2.8.1. Gelation Kinetics.—The dECM pregel was combined with 10% (v/v) medium 199 and neutralized to pH 7.4 to a final concentration of 10.75 mg/mL with 1 M sodium hydroxide. The hydrogel was added to a clear 96-well plate, and the absorbance was read on a plate reader at 37 °C at 560/590 excitation/emission for 45 min. Results were then normalized using eq 3

$$\text{normalized absorbance (NA)} = \frac{\text{Abs}_0 - \text{Abs}}{\text{Abs}_{\text{max}} - \text{Abs}_0} \quad (3)$$

The time to 50 and 95% gelation (NA = 0.5 and 0.95, respectively) were calculated along with the lag time prior to gelation and the speed at which gelation occurred ($R^2 > 0.90$).

2.8.2. Mechanical Properties.—Mechanical properties of the hydrogels were measured via compression test using a rheometer (DHR 2, TA Instruments). Pregels of 12 mg/mL were neutralized to a final concentration of approximately 10.75 mg/mL and molded into cylinders with diameters of 8 mm and heights of 2 mm. Samples were compressed with a load of 250 N in between stainless-steel parallel plates. All tests were performed at a strain rate of 10% of sample height/min until failure at room temperature. The data were collected as a strain (%) versus strain curve (Pa), and the linear elastic modulus of each sample was measured from the slope of the linear region of stresses 5–15%.

2.8.3. Confocal Reflectance Imaging.—The dECM pregel was neutralized, added to PDMS microwells, and incubated at 37 °C for 30–60 min. Samples were imaged with Olympus IX-83 confocal microscope using reflectance imaging, a magnification of 20 \times , and 2 \times digital zoom.

2.9. In Vitro Cultures and Analysis.

2.9.1. 3D Hydrogel Culture.—PDMS microwells were placed into 24-well plates and plasma-cleaned using the Harrick Plasma Expanded Plasma Cleaner for 4 min. Microwells were treated with 1% PEI and 0.2% GA for 10 and 30 min, respectively. The dECM pregel was neutralized (10% medium 199 plus 1 M NaOH), and sNF96.2 cells (passage 4) were

resuspended in volumes equal to medium 199 and embedded at 1 million cells per mL hydrogel. The mixture was added into the treated microwells. Plasma-cleaned PDMS lids were placed on top of the hydrogel, and samples were incubated at 37 °C for 30 min. Complete DMEM with 0.1% forskolin (Schwann cell media) was added to each well, and lids were removed. Gels were cultured for 3 days with a media change after 2 days. On day 3, Live/Dead and alamarBlue assays were performed. Gels were then incubated in FBS-free Schwann cell media overnight, and eluted media was collected on day 4 and concentrated 10-fold. The media were evaluated for brain-derived neurotrophic factor (BDNF), glial cell line-derived neurotrophic factor (GDNF), and nerve growth factor (NGF) content via Luminex assay; values were normalized by dsDNA content. Hydrogels were fixed in 3.7% formaldehyde in PBS for 1 h at 4 °C. Afterward, on a rocker at room temperature, samples were washed three times in PBS for 5 min cycles, 0.05% Triton X-100 in PBS (Triton X-100 solution) for 7 min, and 1% BSA in PBS for 1 h. Hydrogels were incubated with antibodies against S100, GFAP, and Ki67 overnight at 4 °C, rinsed with 0.05% Tween-20 in PBS (Tween-20 solution) three times for 5 min intervals, and incubated with secondary antibodies and DAPI away from light for 1 h. Hydrogels were rinsed with Tween-20 solution and stored in PBS at 4 °C until imaged at 20× magnification with 3.96× digital zoom.

2.9.2. Traditional 2D Culture.—Sterile glass coverslips were coated with poly-L-lysine using 1 mL per 25 cm² for 5 min at room temperature, rinsed in dH₂O, and allowed to dry for 30 min. Ten thousand sNF96.2 cells were seeded onto each coverslip and cultured in Schwann cell media for 3 days. On day 3 of culture, alamarBlue and Live/Dead assays were performed. Cells were treated with FBS-free Schwann cell media overnight, and eluted media was collected on day 4 and concentrated 10-fold. Media was evaluated for BDNF, GDNF, and NGF via Luminex assay. Values were normalized by dsDNA content. Cells were fixed with 3.7% formaldehyde for 10 min at room temperature, washed in 1% BSA/0.1% Tween-20/22.52 mg/mL glycine for 30 min, and stained against S100, GFAP, and Ki67 overnight at 4 °C. Cells were then rinsed in PBS three times for 5 min cycles and incubated with secondary antibodies and DAPI at room temperature for 1 h away from light. Coverslips were rinsed in PBS, mounted using Fluoromount G, and sealed with clear nail polish. Slides were imaged at 20× magnification.

2.10. Peripheral Nerve Disease Model.

PANC-1 human pancreatic ductal adenocarcinoma cells (ATCC CRL-1469) were cultured with complete DMEM until 80–90% confluent. Confluent cells were rinsed with PBS and incubated with serum-free DMEM for 24 h, and the conditioned media were added to 100k MWCO centrifugal filters and concentrated 10-fold to obtain tumor-derived extracellular vesicles (TEVs). The presence of TEVs was confirmed via NanoSight Nanoparticle Tracking Analysis (data not shown) as previously demonstrated.⁵⁹ TEVs were diluted to 1000 per cell and used to treat 3D-cultured Schwann cells for 3 days. Immunofluorescence was performed against S100 and GFAP, and samples were imaged at 20× magnification.

2.11. Image and Statistical Analysis.

Custom MATLAB codes were used to evaluate the percentage of nuclei and collagen remaining in H&E and trichrome images, respectively, as well as saturation per pixel in

alcian blue images. The color histogram feature on Fiji ImageJ was used to analyze the mean pixel intensities of immunofluorescence (i.e., S100, β -III tubulin, collagen I, collagen IV, fibronectin, laminin, CSPG, HSPG, Ki67, and GFAP) and Live/Dead images channels. GraphPad Prism 9.1.0 was utilized to perform unpaired *t*-tests, ordinary one-way and two-way ANOVAS, and Tukey's and Sidak's multiple comparisons tests.

3. RESULTS AND DISCUSSION

3.1. All Decellularization Methods Successfully Removed Cytotoxic Reagents, Apart from Method 3C.

The removal of residual decellularization reagents via wash cycles is essential to avoid cytotoxicity; therefore, each decellularization method explored here implemented PBS washes in the final steps (Figure 1).⁶⁰ Figure 1B describes group assignments for preparation and decellularization methods. Decellularized and fresh nerve-conditioned media were collected and used for sNF96.2 Schwann cell culture. Metabolic activity of the cells was calculated via alamarBlue assay and presented as percent reduction (Figure 2A). A negative percent reduction correlates with increased cell metabolism.

Groups 1A–C, 2A–C, 3A, and 3B had no significant impact on cell metabolism compared to cells cultured with fresh nerve-conditioned media. However, method 3C ($37.33 \pm 20.51\%$) significantly decreased Schwann cell metabolism ($p < 0.05$) over the 2-day culture period. It is likely that the double preparation of these nerves increased chemical penetration via increased surface area, making it difficult to rinse away excess cytotoxic reagents such as Camptothecin. Past studies have used Schwann cells treated with Camptothecin as positive controls for cell apoptosis, so the failure to remove this chemical from the dECM scaffold would be detrimental to cell health in culture.⁶¹ Minimal sciatic nerve preparation, i.e., fat and connective tissue removal only, was indicated in the initial publication of decellularization 3. The authors presented no significant difference in cytotoxicity of decellularized nerves, which is consistent with group 3A and 3B results. This suggests that minimal processing should be used when performing decellularization 3.

3.2. DNA Fragments Were Most Effectively Removed via the SD-Based Method.

Crapo et al. established that remaining DNA levels in dECM should not exceed 50 ng double-stranded (ds) DNA per mg of dry tissue, and the success of each decellularization method relies on adherence to this standard.¹³ It is important to note that fresh and group 1 and 2 nerves were frozen prior to decellularization, which can decrease overall dsDNA content.

Methods 1A (2.30 ± 2.33 ng/mg), 1B (2.69 ± 3.38 ng/mg), and 1C (8.28 ± 6.98 ng/mg) produced nerves with substantial DNA removal well below the standard (Figure 2B). It was found that there is no significant difference in DNA removal between groups 1A, 1B, and 1C. McCrary et al. reported similar findings with preparation.³³ Moreover, there was a significantly lower percentage of nuclei in H&E samples of 1A, 1B, and 1C nerves ($p < 0.0001$), as seen in Figure S1, than in all other decellularized nerve samples except for 3B

nerves (Figure 3A). Groups 2B (24.65 ± 42.94 ng/mg) and 3A (27.85 ± 3.36) also exhibited sufficient DNA removal.

In contrast, there was unsuccessful DNA removal in groups 2A (173.31 ± 69.08 ng/mg), 2C (150.68 ± 192.13 ng/mg), 3B (162.08 ± 59.76 ng/mg), and 3C (76.56 ± 14.20 ng/mg). Surprisingly high DNA content in 2A and 2C can be attributed to a possible false positive reading, as excessive preparation of these nerves may have produced nerves with DNA concentration lower than the kit threshold. H&E samples showed the absence of significant difference between fresh nerves and group 2A, 2B, 2C, 3B, and 3C nerves (Figure 3A). Initial reports of decellularization 2, in which nerves were cut transversely prior to the application of washes, indicated a significant decrease in nuclei versus other methods performed, but values associated with fresh nerve content were unavailable.⁵⁰ Likewise, while decellularization 3 decreased nuclear staining in H&E samples, reported figures revealed remaining cell nuclei in decellularized nerves, which is consistent with our results.⁵¹

As discussed, SD is known for its ability to disrupt the nuclear membrane of cells, thus effectively removing DNA content.⁴⁶ SD has been used previously in conjunction with other detergents and DNase to induce successful removal of genetic material in aortic valve and lung decellularization.^{62,63} This is consistent with the ability of the SD-DNase combination in decellularization 1 to remove dsDNA efficiently. Likewise, decellularization 3 utilizing hypertonic/hypotonic washes was initially performed following only fat and connective tissue removal; authors reported low DNA levels, similar to the results exhibited by group 3A.⁶⁴ A similar approach has produced comparable results in lung decellularization.³⁵ Hypertonic/hypotonic solutions are valued for this quality of efficient DNA removal via cell lysis; however, the over-processed 3B and 3C nerves differed in results.⁶⁴ Shin et al. utilized transverse dissection to prepare nerves for a CHAPS-based decellularization (2B), and the treated nerves were found to have a significant decrease in DNA with this method, which is confirmed here.⁵⁰ However, other studies have shown that CHAPS-based methods leave higher residual DNA content than those of other reagents,^{36,63} which are more consistent with results from our 2A and 2C nerves.

3.3. Retention of ECM Components Varied Across Decellularization Methods.

To create a physiologically relevant model for disease, ECM components should be maintained to mimic the native tissue microenvironment and encourage natural cell phenotype.²¹ To evaluate ECM retention, trichrome (Figure 3B) and alcian blue staining (Figure 3C), as well as immunohistochemistry (IHC) against collagens I and IV, fibronectin, laminin, CSPG, and HSPG were performed (Figure 4). Collagens are the most abundant ECM element in peripheral nerves, providing support and structure for the nerve and modulating essential integrin binding.^{65,66} Additionally, the literature has shown that laminin, CSPG, and HSPG aid in axonal outgrowth while fibronectin supports regeneration following neurological injury.^{65,67} Therefore, it is vital to retain these elements to create a relevant model of peripheral nerve injury and disease. Notably, CSPG has also been investigated for its role in inhibiting regeneration efforts with the onset of nerve injury; this suggests that there is a need to control CSPG content in peripheral nerve models, which

may be investigated further in future studies.^{68,69} For a more comprehensive approach, a proteomic analysis will need to be performed in the future.^{33,70}

Methods 1A–C and 2A–C produced nerves with a significantly increased ($p < 0.0001$) percentage of visible collagen in trichrome samples versus fresh nerves (Figure S1). Additionally, these groups exhibited significantly higher percentages of collagen in trichrome samples ($p < 0.0001$) than methods 3A–C. These results are consistent with the ECM retention previously established in methods 1 and 2. Interestingly, alcian blue samples of method 2B exhibited significantly higher GAG levels ($p < 0.01$) than all other decellularization methods, prompting the continued investigation into GAG protein family contents.

Using analysis of IHC samples, no significant difference was found in collagen I levels between fresh nerves and any decellularization group (Figures 3A,B and S2). However, 1A nerves exhibited significantly different fibronectin levels from fresh nerves ($p < 0.05$) and methods 1B ($p < 0.05$), 1C ($p < 0.05$), and 3A–C ($p < 0.0001$). Method 1A also showed significantly higher fibronectin levels in 1A versus 3B and 3C ($p < 0.0001$), as well as a significant increase in laminin levels from fresh nerves ($p < 0.0001$). However, method 1A showed only moderate HSPG levels compared to methods 2B (ns) and 3A ($p < 0.0001$). CSPG levels of 1A were significantly lower than those of methods 2B ($p < 0.005$), 3A ($p < 0.0001$), and 3C ($p < 0.05$); this is most likely due to the inclusion of ChABC in the SD-based decellularization, though it was found to be less extensive in nerves of preparation A versus those of methods B (ns) and C ($p < 0.05$). Future studies will investigate if this reduction is beneficial to axonal outgrowth and disease modeling applications. Despite this, it is apparent that method 1A significantly preserves the integrity of the ECM, which is also noted by the protocol authors. Additionally, method 2C presented significantly higher collagen IV levels than fresh ($p < 0.001$), 1A ($p < 0.05$), 1B ($p < 0.0001$), 1C ($p < 0.0001$), 2B ($p < 0.005$), 3A ($p < 0.0001$), 3B ($p < 0.0001$), and 3C ($p < 0.05$) nerve. Group 2B nerves had significantly different fibronectin levels than fresh ($p < 0.05$), 1C ($p < 0.05$), 3A ($p < 0.0001$), 3B ($p < 0.0001$), and 3C ($p < 0.0001$) nerves, as well as higher CSPG content compared to methods 2A, 2C, 3A, and 3B and higher HSPG versus methods 1B, 1C, and 3A ($p < 0.05$). The usage of zwitterionic detergents, such as SB-10, SB-16, and CHAPS, could have contributed to increased ECM retention of group 1 and 2 nerves.

In contrast, group 3A nerves exhibited significantly lower ($p < 0.01$) collagen I levels than groups 1A–C and 2C. This disruption of ECM proteins remains consistent for group 3 nerves. While groups 3A–C exhibit no significant difference in collagen IV, fibronectin, or laminin levels than fresh nerves, these levels are lower than those of groups 1 and 2. Alternatively, method 3A showed the most prominent GAG retention according to IHC. While exhibiting lower overall ECM damage, likely due to the long agitation cycles implemented in decellularization, the use of gentle hypertonic/hypotonic solutions may have aided in the retention of native CSPGs and HSPGs by method 3A.³

3.4. Residual Neural Cell Fragments Were Evident in Apoptosis-Induced Tissues.

Finally, IHC against S100 (Schwann cells) and β -III tubulin (neurons) was used to evaluate neural cell removal (Figure 5A–D). Low levels of both S100 and β -III tubulin in fresh nerves

could be contributed to nerve storage at -20°C in PBS and resulting cell death. There was no significant difference in S100 between fresh, 1A–C, and 2A–C nerves (Figure S3). However, S100 levels in fresh nerves were significantly different from groups 3A–C ($p < 0.0001$). Method 1A significantly decreased β -III tubulin levels versus fresh ($p < 0.01$), 1B ($p < 0.0001$), 2A ($p < 0.005$), 2B ($p < 0.01$), 3A ($p < 0.01$), and 3B ($p < 0.0001$) nerves. There was no significant difference in β -III tubulin levels between fresh nerves and methods 1B, 1C, 2A–C, 3A, and 3C, but group 3B presented significantly higher β -III tubulin levels than fresh nerves ($p < 0.05$).

Overall, this analysis suggests that method 1A provides the best neuron cells removal of other decellularization, though not statistically significant from 1C, 2C, and 3C. McCrary et al. showed similarly low levels of β -III tubulin and S100 as well as myelin basic protein.³³ Myelin basic protein was not evaluated in this study; therefore, a more extensive proteomic analysis will need to be performed in the future, as previously stated, to confirm the removal of cellular debris. The lack of neuron removal in 3B could be contributed to the insufficient preparation of the nerve pre-decellularization. While staining of nerves processed before decellularization is unavailable, the initial report showed remaining neurons via neurofilament staining. A significant decrease in cellular content was previously reported; however, this method lacked sufficient removal compared to decellularizations 1 and 2. Residual cell debris could skew *in vitro* analysis of cells embedded in the hydrogels.²⁹

In addition, mean pixel intensities of DAPI channels were also analyzed. While some DAPI signaling may result from dead cells, it is important to consider these levels to account for other possible remaining cell types. Fresh nerves presented significantly higher nuclei levels than 1A–C, 2A–C, and 3A ($p < 0.0001$). Methods 1A and 2C each have significantly lower DAPI signaling than methods 3A ($p < 0.0001$ and $p < 0.01$, respectively), 3B ($p < 0.0001$), and 3C ($p < 0.0001$), and methods 1B, 1C, 2A, and 2B all have significantly different levels than 3B ($p < 0.0001$) and 3C ($p < 0.0001$). Consistent with our results, authors of decellularization 1 and 2 also confirmed successful cell removal via DAPI staining.^{33,50}

3.5. Method 1A is an Optimal Method for Peripheral Nerve dECM Hydrogel Usage.

To determine the best methods and preparations for dECM hydrogel usage, groups were ranked in success in each of the aforementioned experiments. A quantitative 1–9 scale was utilized to evaluate the mean group values from each test, with 1 being the most successful and 9 being the least successful (Table 1). Method 1A received top scores on DNA removal, β -III tubulin levels, DAPI signaling, fibronectin retainment, and laminin levels, method 1B on percentage nuclei in H&E samples and S100 removal (a 3-way tie with 2B and 2C), and method 1C on percentage collagen in trichrome images. Additionally, group 2B nerves had the lowest cytotoxicity and S100 signaling, and method 2C performed best in S100 removal and collagen I and IV levels in IHC images. Finally, method 3A proved most efficient in maintaining ECM GAG content as seen in IHC imaging. The final scores were calculated by summing scores from all tests. Overall, method 1A performed the most successfully with a score of 36; methods 2C (score of 50) and 3A (score of 76) performed in the most ideal manner within their respective decellularization methods. Method 1A provided

the ideal amount of preparation to allow the utilized anionic and zwitterionic detergents to remove cellular debris while maintaining ECM integrity. McCrary et al. utilized this preparation in the original method and produced similar results.³³ This method has shown success in hydrogel preparation,⁷¹ which is necessary for the disease modeling application aimed for here. Both methods 2 and 3 have been implemented in tissue-engineered scaffold preparation; therefore, the efficacies of 2C and 3A as dECM hydrogels were evaluated versus that of 1A.

After decellularization, nerves were lyophilized and digested into pregel solutions at 12 mg/mL (Figure 6A). Pregels were neutralized to a concentration of 10.75 mg/mL, and rheological characterization (Figure 6B), gelation kinetics (Figure 6C), and collagen fibril assembly (Figure 6D) were assessed for each variation. The 1A hydrogel was found to be significantly stiffer ($E = 396.99 \pm 26.06$ Pa) than 2C ($E = 142.42 \pm 29.63$ Pa) and 3A gels ($E = 240.29 \pm 38.61$ Pa). Though rheology is underutilized in assessing peripheral nerve elastic moduli due to the soft mechanical characteristics, the elastic modulus of the 1A hydrogel better mimics the properties of peripheral nerves than 2C and 3A hydrogels, according to alternative compression and indentation methods.^{66,72} Future studies will establish the storage and loss moduli of this hydrogel to confirm its viscoelastic properties.

In evaluating the change in absorbance mediated by collagen fibril assembly in gelation kinetics, the method 2C hydrogel achieved 50 and 95% gelation most quickly and with the fastest rate (established by the slope of the linear gelation curve). Method 3A produced a hydrogel that reaches 50 and 95% gelation the slowest among the three evaluated, while the 1A hydrogel polymerized at the slowest rate. Notably, although 2C and 3A hydrogels showed the two highest gelation speeds, the resulting gels were very soft, as evident by the calculated elastic moduli, and may be difficult to use in disease modeling applications. Both 1A and 2C hydrogels reach their gelation periods around 10 min, which is replicated in the literature.⁷¹ To further analyze collagen fibrillogenesis, confocal reflectance imaging was performed on each hydrogel. The 2C and 3A hydrogels formed medium and long fibers, respectively, while 1A fibers were more densely packed though not as prominent. Nevertheless, the high density of 1A hydrogels may correlate with its relatively higher stiffness, which produces a more physiologically relevant model of peripheral nerve anatomy.⁷³ Therefore, the SD-based decellularization with nerve epineurial removal was implemented in hydrogel fabrication moving forward.

3.6. The Produced dECM Hydrogel Successfully Maintains a Physiologically Relevant Schwann Cell Culture.

Hydrogel culture of Schwann cells was performed and compared to cells cultured on a poly-L-lysine-coated coverslip. It is important to note that sNF96.2 human Schwann-like cells are derived from malignant peripheral nerve sheath tumors;⁷⁴ future studies using myelinating Schwann cells should be performed to evaluate as a more comprehensively relevant platform for disease modeling. Schwann cells were embedded and seeded at 10,000 cells per 324 mm² coverslip or 1 million cells per mL hydrogel. After 3 days of culture, alamarBlue (Figure 7A) and Live/Dead (Figure 7B) assays were performed. It was found that there was no significant difference in cell metabolism via alamarBlue

of 2D-cultured versus 3D-cultured cells nor change in viability according to Live/Dead samples. These assessments validate the capability of the hydrogel to maintain a healthy cell culture. Immunofluorescence was performed against proliferation marker Ki67 (Figure 7C); monolayer-cultured Schwann cells had significantly higher Ki67 levels compared to those in 3D ($p < 0.05$). This phenomenon is widely accepted and evident in the literature and more closely mimics cell activity *in vivo* than traditional 2D cultures.^{75–77}

Cells were also incubated overnight with serum-free DMEM, and Luminex assays were run to assess NGF, BDNF, and GDNF secretion (Figure 7D). These cytokines are expressed by Schwann cells in response to an injury and therefore should not be highly expressed by Schwann cells under physiological conditions.^{78–81} These assays showed that Schwann cells cultured in 2D exhibited significantly higher NGF ($p < 0.005$), BDNF ($p < 0.0001$), and GDNF ($p < 0.05$) levels than Schwann cells cultured in the dECM hydrogel. The literature shows that monolayer cultures alter cellular phenotype and biochemical factors, including gene and protein expression; therefore, the increased secretome related to nerve injury and disease activation should be expected in 2D-cultured Schwann cells.⁸² Overall, this suggests that 3D-cultured Schwann cells act in a more physiologically relevant manner than those in 2D culture, presenting an advantage of utilizing these dECM hydrogels for disease modeling applications.

3.7. The dECM Hydrogel May Be Implemented in Modeling Peripheral Nerve Disorders *In Vitro*.

Schwann cells have been implicated in the progression of pancreatic cancer perineural invasion, in which they draw cancer cells toward adjacent nerve tissue to promote invasion and metastasis to secondary sites.⁸³ Within the last decade, TEVs have been acknowledged in their ability to facilitate cancer aggressiveness and are established promoters of cancer–nerve crosstalk.⁸⁴ Here, 3D-cultured Schwann cells were treated with PANC-1 human pancreatic ductal adenocarcinoma tumor-derived extracellular vesicles (TEV) for a 3-day period to confirm the ability of our dECM hydrogel to allow for *in vitro* disease modeling.

Following culture, control and treated cell-laden hydrogels as well as 2D-cultured Schwann cells were evaluated via immunofluorescence of S100 (physiological Schwann cells) and GFAP (activated Schwann cells). Though analysis (Figure 7E) highlights the increase in GFAP to S100 ratio in 2D culture versus control 3D culture (ns), monolayer-cultured cells inefficiently present in a repair phenotype-like manner of which Schwann cells enter upon injury and disease onset. However, 3D-cultured Schwann cells treated with TEVs (1000 TEVs per Schwann cell) show significant changes in their GFAP to S100 versus both monolayer- ($p < 0.005$) and untreated 3D-cultured Schwann cells ($p < 0.0001$). Elevated GFAP levels in mature Schwann cells *in vivo* is correlated with activation following pathophysiological events, such as peripheral nerve injury and cancer invasion.^{79,80,85} While this relationship has been speculated, there exists limited evidence that TEVs modulate the Schwann cell activation necessary for the onset of perineural invasion.⁸⁶ Future studies will investigate specific mechanisms of TEV-mediated Schwann cell activation in cancer settings. Changes to cell behavior in 2D versus 3D is also evident in dorsal root ganglia neurite cultures, signifying an important characteristic this hydrogel achieves to act as a biomimetic

testbed.⁸⁷ Overall, this observation establishes the ability of this dECM hydrogel to facilitate natural, quiescent Schwann cell behavior as well as its ability to be used in *in vitro* disease modeling applications.

4. CONCLUSIONS

Here, we established that SD-based decellularization in combination with epineurium removal is optimal for peripheral nerve ECM hydrogel fabrication. The decellularization established by McCrary et al. effectively removed cellular debris, retained ECM content, and produced biocompatible scaffolds. In addition, the resulting dECM hydrogel maintained physiological mechanical properties compared to hydrogels fabricated with alternative decellularization methods. The dECM hydrogel was then concluded to be a viable option for the quiescent 3D culture of Schwann cells as well as offering a platform for successful disease modeling. This comparative study establishes a standard for peripheral nerve decellularization that will allow for the more physiologically relevant study of peripheral nerve disease than previous 2D studies. Such studies will produce more clinically translatable conclusions for future treatment options. With the optimal decellularization method established, future work will include further evaluation of the biomechanical properties of the hydrogel, more in-depth evaluation of Schwann cell polarity in 3D culture, and continued analysis of Schwann cell-related disease modeling, e.g., peripheral nerve injury and cancer invasion.^{88–91}

Supplementary Material

Refer to Web version on PubMed Central for supplementary material.

ACKNOWLEDGMENTS

This project was funded by the National Institutes of Health through award number P20GM139768, PhRMA Foundation, Arkansas Biosciences Institute, and University of Arkansas Women's Giving Circle, all awarded to Y.H.S. The authors thank Dr. Jeffrey Wolchok for the donation of animals. For access to vital equipment, the authors thank Dr. Kartik Balachandran, Dr. Raj Rao, and Dr. Jin-Woo Kim at the University of Arkansas.

REFERENCES

- (1). Yue B Biology of the Extracellular Matrix: An Overview. *J. Glaucoma* 2014, S20–S23. [PubMed: 25275899]
- (2). Freytes DO; Martin J; Velankar SS; Lee AS; Badylak SF Preparation and rheological characterization of a gel form of the porcine urinary bladder matrix. *Biomaterials* 2008, 29, 1630–1637. [PubMed: 18201760]
- (3). Mendibil U; Ruiz-Hernandez R; Retegi-Carrion S; Garcia-Urquia N; Olalde-Graells B; Abarrategi A Tissue-specific decellularization methods: Rationale and strategies to achieve regenerative compounds. *Int. J. Mol. Sci* 2020, 21, No. 5447. [PubMed: 32751654]
- (4). Frantz C; Stewart KM; Weaver VM The extracellular matrix at a glance. *J. Cell Sci* 2010, 123, 4195–4200. [PubMed: 21123617]
- (5). Gordon MK; Hahn RA Collagens. *Cell Tissue Res* 2010, 339, 247–257. [PubMed: 19693541]
- (6). Ishihara J; Ishihara A; Fukunaga K; Sasaki K; White MJV; Briquez PS; Hubbell JA Laminin heparin-binding peptides bind to several growth factors and enhance diabetic wound healing. *Nat. Commun* 2018, 9, No. 2163. [PubMed: 29867149]

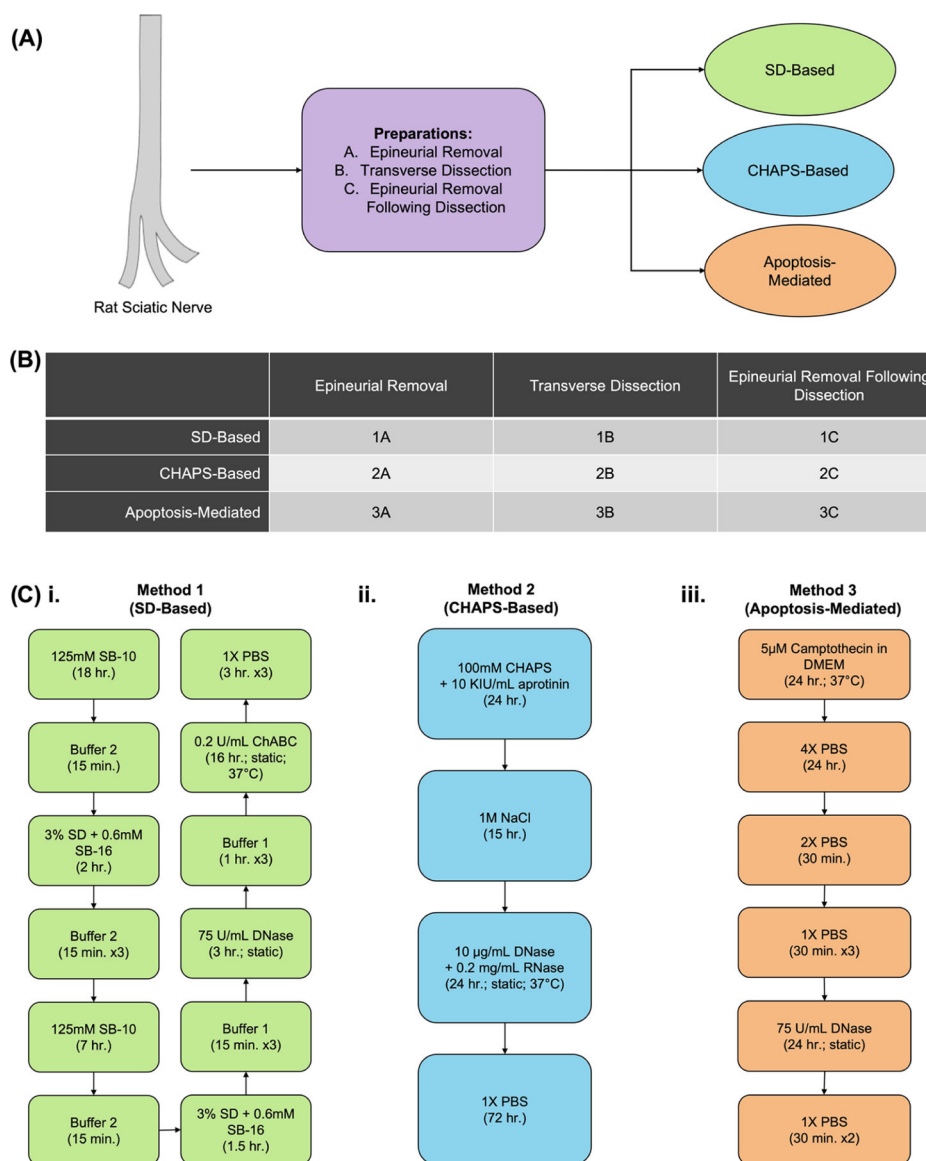
- (7). Smock RG; Meijers R Roles of glycosaminoglycans as regulators of ligand/receptor complexes. *Open Biol* 2018, 8, No. 180026. [PubMed: 30282658]
- (8). Karamanos NK; Theocharis AD; Piperigkou Z; Manou D; Passi A; Skandalis SS; Vynios DH; Orian-Rousseau V; Ricard-Blum S; Schmelzer CEH; Duca L; Durbee M; Afratis NA; Troeberg L; Franchi M; Masola V; Onisto M A guide to the composition and functions of the extracellular matrix. *FEBS J* 2021, 288, 6850–6912. [PubMed: 33605520]
- (9). Egeblad M; Rasch MG; Weaver VM Dynamic interplay between the collagen scaffold and tumor evolution. *Curr. Opin. Cell Biol* 2010, 22, 697–706. [PubMed: 20822891]
- (10). Xue M; Jackson CJ Extracellular Matrix Reorganization During Wound Healing and Its Impact on Abnormal Scarring. *Adv. Wound Care* 2015, 4, 119–136.
- (11). Nelson CM; Bissell MJ Of Extracellular Matrix, Scaffolds, and Signaling. *Annu. Rev. Cell Dev. Biol* 2006, 22, 287–309. [PubMed: 16824016]
- (12). Sung KE; Su X; Berthier E; Pehlke C; Friedl A; Beebe DJ Understanding the Impact of 2D and 3D Fibroblast Cultures on In Vitro Breast Cancer Models. *PLoS One* 2013, 8, No. e76373. [PubMed: 24124550]
- (13). Crapo PM; Medberry CJ; Reing JE; Tottey S; van der Merwe Y; Jones KE; Badylak SF Biologic scaffolds composed of central nervous system extracellular matrix. *Biomaterials* 2012, 33, 3539–3547. [PubMed: 22341938]
- (14). Wang C; Tang Z; Zhao Y; Yao R; Li L; Sun W Threedimensional in vitro cancer models: A short review. *Biofabrication* 2014, 6, No. 022001. [PubMed: 24727833]
- (15). Qiao H; Tang T Engineering 3D Approaches to Model the Dynamic Microenvironments of Cancer Bone Metastasis. *Bone Res* 2018, 6, No. 3. [PubMed: 29507817]
- (16). Chiou AE; Fischbach C Tissue-Engineered Models for Studies of Bone Metastasis. In *Tumor Organoids; Cancer Drug Discovery and Development*; Humana Press, 2018; pp 35–49.
- (17). Takai A; Fako V; Dang H; Forgues M; Yu Z; Budhu A; Wang XW Three-dimensional Organotypic Culture Models of Human Hepatocellular Carcinoma. *Sci. Rep* 2016, 6, No. 21174. [PubMed: 26880118]
- (18). Ferreira GS; Veening-Griffioen DH; Boon WPC; Moors EHM; van Meer PJK Levelling the translational gap for animal to human efficacy data. *Animals* 2020, 10, No. 1199. [PubMed: 32679706]
- (19). Seyhan AA Lost in translation: the valley of death across preclinical and clinical divide – identification of problems and overcoming obstacles. *Transl. Med. Commun* 2019, 4, No. 18.
- (20). Katt ME; Placone AL; Wong AD; Xu ZS; Searson PC In vitro tumor models: Advantages, disadvantages, variables, and selecting the right platform. *Front. Bioeng. Biotechnol* 2016, 4, No. 12. [PubMed: 26904541]
- (21). McCrary MW; Bousalis D; Mobini S; Song YH; Schmidt CE Decellularized tissues as platforms for in vitro modeling of healthy and diseased tissues. *Acta Biomater* 2020, 111, 1–19. [PubMed: 32464269]
- (22). Hoshiba T; YaMaoka T Extracellular Matrix Scaffolds for Tissue Engineering and Biological Research. In *Decellularized Extracellular Matrix: Characterization, Fabrication and Applications*; Royal Society of Chemistry, 2020; pp 3–14.
- (23). Berthiaume F; Maguire TJ; Yarmush ML Tissue engineering and regenerative medicine: History, progress, and challenges. *Annu. Rev. Chem. Biomol. Eng* 2011, 2, 403–430. [PubMed: 22432625]
- (24). Buckenmeyer MJ; Meder TJ; Prest TA; Brown BN Decellularization techniques and their applications for the repair and regeneration of the nervous system. *Methods* 2020, 171, 41–61. [PubMed: 31398392]
- (25). Garreta E; Oria R; Tarantino C; Pla-Roca M; Prado P; Fernández-Avilés F; Campistol JM; Samitier J; Montserrat N Tissue engineering by decellularization and 3D bioprinting. *Mater. Today* 2017, 20, 166–178.
- (26). Fernández-Pérez J; Ahearne M The impact of decellularization methods on extracellular matrix derived hydrogels. *Sci. Rep* 2019, 9, No. 14933. [PubMed: 31624357]

- (27). Gregory E; Dugan R; David G; Song YH The biology and engineered modeling strategies of cancer-nerve crosstalk. *Biochim. Biophys. Acta, Rev. Cancer* 2020, 1874, No. 188406. [PubMed: 32827578]
- (28). Parmaksiz M; Dogan A; Odabas S; Elçin AE; Elçin YM Clinical applications of decellularized extracellular matrices for tissue engineering and regenerative medicine. *Biomed. Mater* 2016, 11, No. 022003. [PubMed: 26989100]
- (29). Gilbert TW; Sellaro TL; Badylak SF Decellularization of tissues and organs. *Biomaterials* 2006, 27, 3675–3683. [PubMed: 16519932]
- (30). Doblado LR; Martínez-Ramos C; Pradas MM Biomaterials for Neural Tissue Engineering. *Front. Nanotechnol* 2021, v, No. 643507.
- (31). Watanabe N; Mizuno M; Matsuda J; Nakamura N; Otabe K; Katano H; Ozeki N; Kohno Y; Kimura T; Tsuji K; Koga H; Kishida A; Sekiya I Comparison of High-Hydrostatic-Pressure Decellularized Versus Freeze-Thawed Porcine Menisci. *J. Orthop. Res* 2019, 37, 2466–2475. [PubMed: 31115925]
- (32). Seo Y; Jung Y; Kim SH Decellularized heart ECM hydrogel using supercritical carbon dioxide for improved angiogenesis. *Acta Biomater* 2018, 67, 270–281. [PubMed: 29223704]
- (33). McCrary MW; Vaughn NE; Hlavac N; Song YH; Wachs RA; Schmidt CE Novel Sodium Deoxycholate-Based Chemical Decellularization Method for Peripheral Nerve. *Tissue Eng., Part C* 2020, 26, 23–36.
- (34). Hillebrandt KH; Everwien H; Haep N; Keshi E; Pratschke J; Sauer IM Strategies based on organ decellularization and recellularization. *Transplant Int* 2019, 32, 571–585.
- (35). Song YH; Maynes MA; Hlavac N; Visosevic D; Daramola KO; Porvasnik SL; Schmidt CE Development of novel apoptosis-assisted lung tissue decellularization methods. *Biomater. Sci* 2021, 9, 3485–3498. [PubMed: 33949462]
- (36). White LJ; Taylor AJ; Faulk DM; Keane TJ; Saldin LT; Reing JE; Swinehart IT; Turner NJ; Ratner BD; Stephen F The impact of detergents on the tissue decellularization process: aToF-SIMS study. *Acta Biomater* 2017, 50, 207–219. [PubMed: 27993639]
- (37). Seddon AM; Curnow P; Booth PJ Membrane proteins, lipids and detergents: Not just a soap opera. *Biochim. Biophys. Acta, Biomembr* 2004, 1666, 105–117.
- (38). Kim JK; Koh YD; Kim JO; Seo DH Development of a decellularization method to produce nerve allografts using less invasive detergents and hyper/hypotonic solutions. *J. Plast. Reconstr. Aesthetic Surg* 2016, 69, 1690–1696.
- (39). Bourguin PE; Gaudiello E; Pippenger B; Jaquier C; Klein T; Pigeot S; Todorov A; Feliciano S; Banfi A; Martin I Engineered Extracellular Matrices as Biomaterials of Tunable Composition and Function. *Adv. Funct. Mater* 2017, 27, No. 1605486.
- (40). Madhusudanan P; Raju G; Shankarappa S Hydrogel systems and their role in neural tissue engineering. *J. R. Soc., Interface* 2020, 17, No. 20190505. [PubMed: 31910776]
- (41). Caliri SR; Burdick JA A Practical Guide to Hydrogels for Cell Culture. *Nat. Methods* 2016, 13, 405–414. [PubMed: 27123816]
- (42). Slaughter BV; Khurshid S; Fisher O; Khademhosseini A; Peppas N Hydrogels in Regenerative Medicine. *Adv. Mater* 2009, 21, 3307–3329. [PubMed: 20882499]
- (43). Sackett SD; Tremmel DM; Ma F; Feeney AK; Maguire RM; Brown ME; Zhou Y; Li X; O'Brien C; Li L; Burlingham WJ; Odorico JS Extracellular matrix scaffold and hydrogel derived from decellularized and delipidized human pancreas. *Sci. Rep* 2018, 8, No. 10452. [PubMed: 29993013]
- (44). Lin T; Liu S; Chen S; Qiu S; Rao Z; Liu J; Zhu S; Yan L; Mao H; Zhu Q; Quan D; Liu X Hydrogel derived from porcine decellularized nerve tissue as a promising biomaterial for repairing peripheral nerve defects. *Acta Biomater* 2018, 73, 326–338. [PubMed: 29649641]
- (45). Wolf MT; Daly KA; Brennan-pierce EP; Johnson SA; Carruthers C; Amore AD; Nagarkar SP; Sachin S; Badylak SF A Hydrogel Derived From Decellularized Dermal Extracellular Matrix. *Biomaterials* 2012, 33, 7028–7038. [PubMed: 22789723]
- (46). Gilpin A; Yang Y Decellularization Strategies for Regenerative Medicine: From Processing Techniques to Applications. *BioMed Res. Int* 2017, 2017, No. 9831534. [PubMed: 28540307]

- (47). Meder T; Prest T; Skillen C; Marchal L; Yupanqui VT; Soletti L; Gardner P; Cheetham J; Brown BN Nerve-specific extracellular matrix hydrogel promotes functional regeneration following nerve gap injury. *npj Regener. Med* 2021, 6, No. 69.
- (48). Nietzer S; Baur F; Sieber S; Hansmann J; Schwarz T; Stoffer C; Häfner H; Gasser M; Waaga-Gasser AM; Walles H; Dandekar G Mimicking Metastases Including Tumor Stroma: A New Technique to Generate a Three-Dimensional Colorectal Cancer Model Based on a Biological Decellularized Intestinal Scaffold. *Tissue Eng., Part C* 2016, 22, 621–635.
- (49). Dunne LW; Huang Z; Meng W; Fan X; Zhang N; Zhang Q; An Z Human decellularized adipose tissue scaffold as a model for breast cancer cell growth and drug treatments. *Biomaterials* 2014, 35, 4940–4949. [PubMed: 24661550]
- (50). Shin YH; Park SY; Kim JK Comparison of systematically combined detergent and nuclease-based decellularization methods for acellular nerve graft: An ex vivo characterization and in vivo evaluation. *J. Tissue Eng. Regener. Med* 2019, 13, 1241–1252.
- (51). Cornelison RC; Wellman SM; Park JH; Porvasnik SL; Song YH; Wachs RA; Schmidt CE Development of an Apoptosis-Assisted Decellularization Method for Maximal Preservation of Nerve Tissue Structure: Apoptosis-Assisted Decellularization for Maximal Nerve Tissue Preservation. *Physiol. Behav* 2017, 176, 139–148. [PubMed: 28363838]
- (52). Kasper M; Deister C; Beck F; Schmidt CE Bench-to-Bedside Lessons Learned: Commercialization of an Acellular Nerve Graft. *Adv. Healthcare Mater* 2020, 9, No. 2000174.
- (53). Han G-H; Peng J; Wang Y; et al. Therapeutic strategies for peripheral nerve injury: decellularized nerve conduits and Schwann cell transplantation. *Neural Regener. Res* 2019, 14, 1343–1351.
- (54). Lovati AB; D'Arrigo D; Odella S; Tos P; Geuna S; Raimondo S Nerve repair using decellularized nerve grafts in rat models. A review of the literature. *Front. Cell. Neurosci* 2018, 12, No. 427. [PubMed: 30510503]
- (55). Wang ZZ; Sakiyama-Elbert SE Matrices, scaffolds & carriers for cell delivery in nerve regeneration. *Exp. Neurol* 2019, 319, No. 112837. [PubMed: 30291854]
- (56). Boni R; Ali A; Shavandi A; Clarkson AN Current and novel polymeric biomaterials for neural tissue engineering. *J. Biomed. Sci* 2018, 25, No. 90. [PubMed: 30572957]
- (57). Sharma AD; McCoy L; Jacobs E; Willey H; Behn JQ; Nguyen H; Bolon B; Curley JL; Moore MJ Engineering a 3D functional human peripheral nerve in vitro using the Nerve-on-a-Chip platform. *Sci. Rep* 2019, 9, No. 8921. [PubMed: 31222141]
- (58). Song YH; Shon SH; Shan M; Stroock AD; Fischbach C Adipose-derived stem cells increase angiogenesis through matrix metalloproteinase-dependent collagen remodeling. *Integr. Biol* 2016, 8, 205–215.
- (59). Song YH; Warncke C; Choi SJ; Choi S; Chiou AE; Ling L; Liu HY; Daniel S; Antonyak MA; Cerione RA; Fischbach C Breast Cancer-Derived Extracellular Vesicles Stimulate Myofibroblast Differentiation and Pro-Angiogenic Behavior of Adipose Stem Cells. *Matrix Biol* 2017, 60–61, 190–205.
- (60). Gilpin A; Yang Y Decellularization Strategies for Regenerative Medicine: From Processing Techniques to Applications. *BioMed Res. Int* 2017, 2017, No. 9831534. [PubMed: 28540307]
- (61). Tapinos N; Rambukkana A Insights into regulation of human Schwann cell proliferation by Erk1/2 via a MEK-independent and p56Lck-dependent pathway from leprosy bacilli. *Proc. Natl. Acad. Sci. U.S.A* 2005, 102, 9188–9193. [PubMed: 15967991]
- (62). Liu X; Li N; Gong D; Xia C; Xu Z Comparison of detergent-based decellularization protocols for the removal of antigenic cellular components in porcine aortic valve. *Xenotransplantation* 2018, 25, No. e12380. [PubMed: 29446183]
- (63). Gilpin SE; Guyette JP; Gonzalez G; Ren X; Asara JM; Mathisen DJ; Vacanti JP; Ott HC Perfusion decellularization of human and porcine lungs: Bringing the matrix to clinical scale. *J. Heart Lung Transplant* 2014, 33, 298–308. [PubMed: 24365767]
- (64). Crapo PM; Gilbert TW; Badylak SF An overview of tissue and whole organ decellularization processes. *Biomaterials* 2011, 32, 3233–3243. [PubMed: 21296410]
- (65). Plantman S Proregenerative properties of ECM molecules. *BioMed Res. Int* 2013, 2013, No. 981695. [PubMed: 24195084]

- (66). Rosso G; Guck J Mechanical changes of peripheral nerve tissue microenvironment and their structural basis during development. *APL Bioeng* 2019, 3, No. 036107. [PubMed: 31893255]
- (67). Condomitti G; De Wit J Heparan sulfate proteoglycans as emerging players in synaptic specificity. *Front. Mol. Neurosci* 2018, 11, No. 14. [PubMed: 29434536]
- (68). Zou JL; Sun JH; Qiu S; Chen SH; He FL; Li JC; Mao HQ; Liu XL; Quan DP; Zeng YS; Zhu QT Spatial distribution affects the role of CSPGs in nerve regeneration via the actin filament-mediated pathway. *Exp. Neurol* 2018, 307, 37–44. [PubMed: 29852179]
- (69). Siebert JR; Conta Steencken A; Osterhout DJ Chondroitin Sulfate Proteoglycans in the Nervous System: Inhibitors to Repair. *BioMed Res. Int* 2014, 2014, No. 845323. [PubMed: 25309928]
- (70). Byron A; Humphries JD; Humphries MJ Defining the extracellular matrix using proteomics. *Int. J. Exp. Pathol* 2013, 94, 75–92. [PubMed: 23419153]
- (71). Bousalis D; McCrary MW; Vaughn N; Hlavac N; Evering A; Kolli S; Song YH; Morley C; Angelini T; Schmidt CE Decellularized peripheral nerve as an injectable delivery vehicle for neural applications. *J. Biomed. Mater. Res., Part A* 2022, 110, 595–611.
- (72). Paggi V; Akouissi O; Micera S; Lacour SP Compliant peripheral nerve interfaces. *J. Neural Eng* 2021, 18, No. 031001. [PubMed: 33750743]
- (73). Ju MS; Lin CCK; Chang CT Researches on biomechanical properties and models of peripheral nerves - A review. *J. Biomech. Sci. Eng* 2017, 12, No. 16–00678.
- (74). Li Y; Rao PK; Wen R; Song Y; Muir D; Wallace P; Van Horne SJ; Tennekoon GI; Kadesch T Notch and Schwann cell transformation. *Oncogene* 2004, 23, 1146–1152. [PubMed: 14762442]
- (75). Kapałczy ska M; Kolenda T; Przybyła W; Zaj czkowska M; Teresiak A; Filas V; Ibbs M; Bli niak R; Luczewski Ł; Lamperska K 2D and 3D cell cultures – a comparison of different types of cancer cell cultures. *Arch. Med. Sci* 2016, 14, 910–919. [PubMed: 30002710]
- (76). Powell R; Eleftheriadou D; Kellaway S; Phillips JB Natural Biomaterials as Instructive Engineered Microenvironments That Direct Cellular Function in Peripheral Nerve Tissue Engineering. *Front. Bioeng. Biotechnol* 2021, 9, No. 674473. [PubMed: 34113607]
- (77). Melissaridou S; Wiechec E; Magan M; Jain MV; Chung MK; Farnebo L; Roberg K The effect of 2D and 3D cell cultures on treatment response, EMT profile and stem cell features in head and neck cancer. *Cancer Cell Int* 2019, 19, No. 16. [PubMed: 30651721]
- (78). Bampton ETW; Taylor JSH Effects of Schwann cell secreted factors on PC12 cell neuritogenesis and survival. *J. Neurobiol* 2005, 63, 29–48. [PubMed: 15702477]
- (79). Jessen KR; Mirsky R The success and failure of the schwann cell response to nerve injury. *Front. Cell. Neurosci* 2019, 13, No. 33. [PubMed: 30804758]
- (80). Deborde S; Wong RJ How Schwann cells facilitate cancer progression in nerves. *Cell. Mol. Life Sci* 2017, 74, 4405–4420. [PubMed: 28631007]
- (81). Ladak A; Olson J; Tredget EE; Gordon T Differentiation of mesenchymal stem cells to support peripheral nerve regeneration in a rat model. *Exp. Neurol* 2011, 228, 242–252. [PubMed: 21281630]
- (82). Kim YE; Jeon HJ; Kim D; Lee SY; Kim KY; Hong J; Maeng PJ; Kim KR; Kang D Quantitative Proteomic Analysis of 2D and 3D Cultured Colorectal Cancer Cells: Profiling of Tankyrase Inhibitor XAV939-Induced Proteome. *Sci. Rep* 2018, 8, No. 13255. [PubMed: 30185973]
- (83). Deborde S; Omelchenko T; Lyubchik A; Zhou Y; He S; McNamara WF; Chernichenko N; Lee SY; Barajas F; Chen CH; Bakst RL; Vakiani E; He S; Hall A; Wong RJ Schwann cells induce cancer cell dispersion and invasion. *J. Clin. Invest* 2016, 126, 1538–1554. [PubMed: 26999607]
- (84). Liu X; Yang X; Zhan C; Zhang Y; Hou J; Yin X Perineural Invasion in Adenoid Cystic Carcinoma of the Salivary Glands: Where We Are and Where We Need to Go. *Front. Oncol* 2020, 10, No. 1493. [PubMed: 33014792]
- (85). Liu B; Xin W; Tan JR; Zhu RP; Li T; Wang D; Kan SS; Xiong DK; Li HH; Zhang MM; Sun HH; Wagstaff W; Zhou C; Wang ZJ; Zhang YG; He TC Myelin sheath structure and regeneration in peripheral nerve injury repair. *Proc. Natl. Acad. Sci. U.S.A* 2019, 116, 22347–22352. [PubMed: 31611410]
- (86). Hussain Z; Nigri J; Tomasini R The cellular and biological impact of extracellular vesicles in pancreatic cancer. *Cancers* 2021, 13, No. 3040. [PubMed: 34207163]

- (87). Kofron CM; Fong VJ; Hoffman-Kim D Neurite outgrowth at the interface of 2D and 3D growth environments. *J. Neural Eng* 2009, 6, No. 016002. [PubMed: 19104140]
- (88). Park SE; Ahn J; Jeong HE; Youn I; Huh D; Chung S A three-dimensional in vitro model of the peripheral nervous system. *NPG Asia Mater* 2021, 13, No. 2.
- (89). Zou JL; Liu S; Sun JH; Yang WH; Xu YW; Rao ZL; Jiang B; Zhu QT; Liu XL; Wu JL; Chang C; Mao HQ; Ling EA; Quan DP; Zeng YS Peripheral Nerve-Derived Matrix Hydrogel Promotes Remyelination and Inhibits Synapse Formation. *Adv. Funct. Mater* 2018, 28, No. 1705739.
- (90). Gingras M; Bergeron J; Déry J; Durham HD; Berthod F In vitro development of a tissue-engineered model of peripheral nerve regeneration to study neurite growth. *FASEB J* 2003, 17, 1–16. [PubMed: 12522106]
- (91). Zhang PX; Han N; Kou YH; Zhu QT; Liu XL; Quan DP; Chen JG; Jiang BG Tissue engineering for the repair of peripheral nerve injury. *Neural Regener. Res* 2019, 14, 51–58.

**Figure 1.**

Decellularization methods. Prior to application, murine sciatic nerves were prepared via epineurial removal and/or dissection in half. (A) Sodium deoxycholate (SD)-based decellularization was supplemented with washes of SB-10, 100 mM sodium/50 mM phosphate buffer (buffer 2), DNase, 50 mM sodium/10 mM phosphate buffer (buffer 1), and chondroitinase ABC (ChABC). (B) 3-((3-Cholamidopropyl)dimethylammonio)-1-propanesulfonate (CHAPS)-based decellularization was performed with CHAPS/aprotinin, sodium chloride (NaCl), DNase, and RNase washes. (C) Apoptosis-targeted decellularization utilized washes of Camptothecin in Dulbecco's modified Eagle's medium (DMEM), decreasing concentrations of PBS, and DNase treatment.

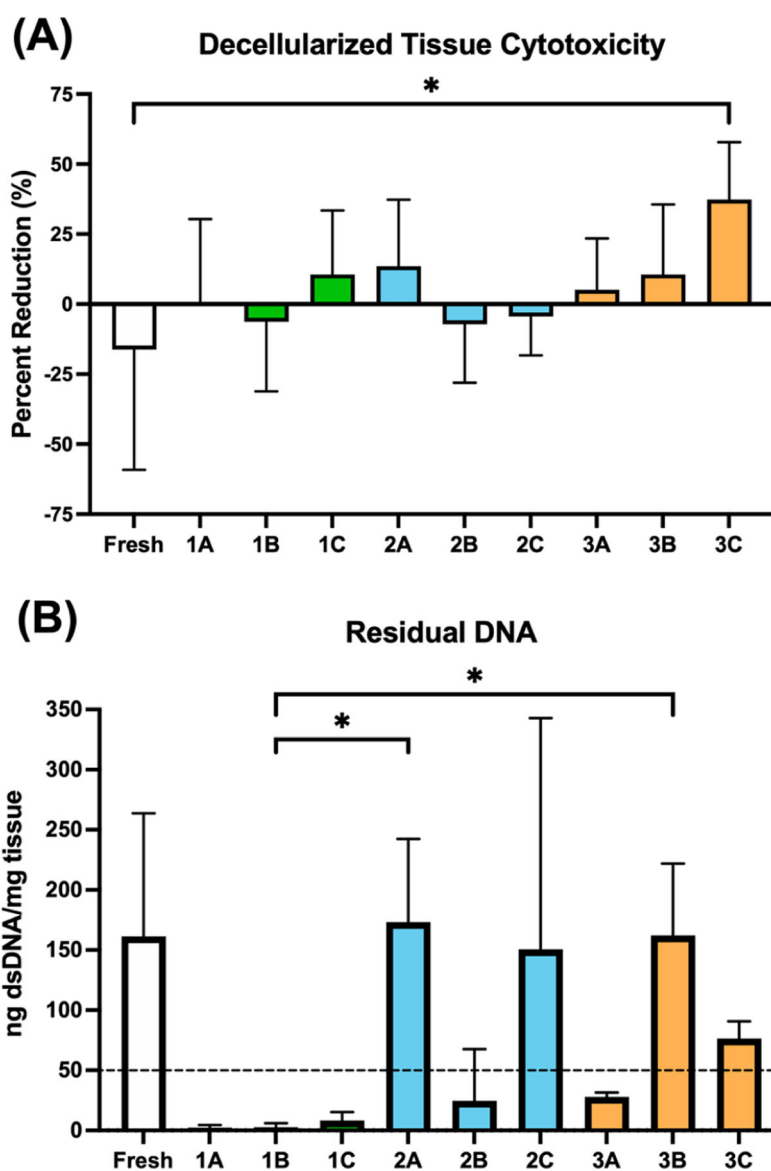


Figure 2. DNA analysis and cytotoxicity of decellularized nerves. (A) Decellularized nerves were soaked in DMEM, and the media collected was used for Schwann cell culture. Cell metabolism was analyzed via percent reduction with an alamarBlue assay ($n = 6$). (B) Residual DNA from fresh and decellularized sciatic nerves was isolated ($n = 3$), and concentration was computed. The dotted line indicates established acceptable levels (50 ng/mg tissue) of residual DNA in decellularized tissues.¹³ Ordinary one-way ANOVAs and Tukey's multiple comparisons tests were performed (A, B) with GraphPad Prism 9.1.0. * $p < 0.05$.

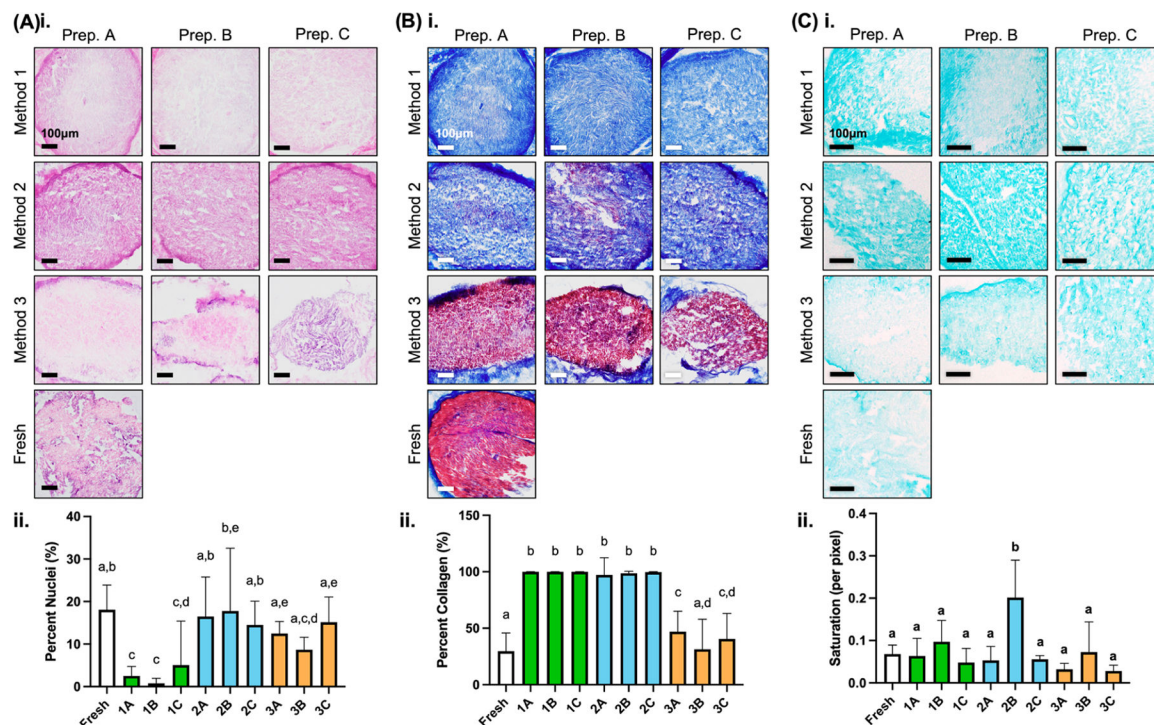
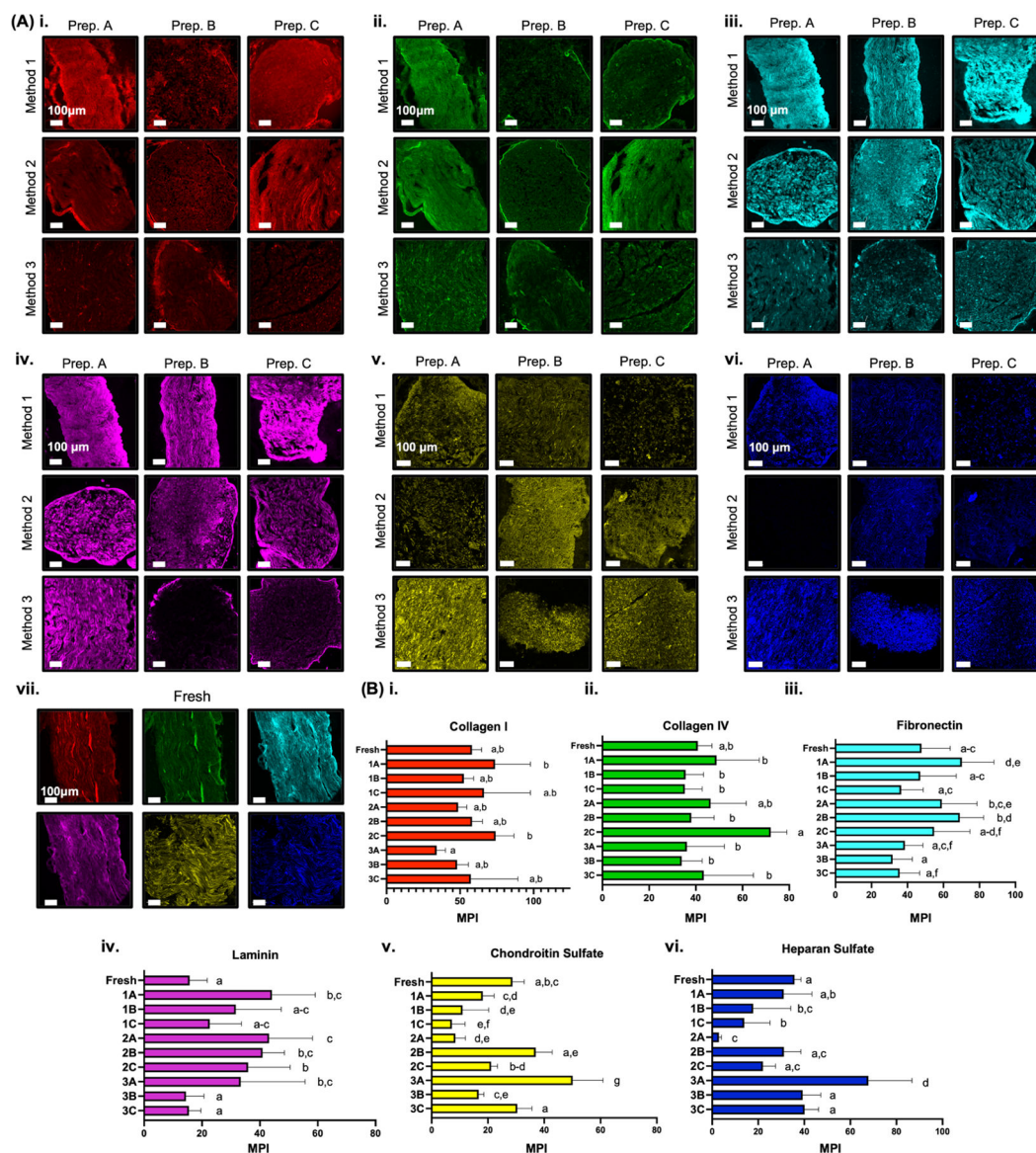


Figure 3.

Histological evaluation of decellularized sciatic nerves. H&E (A(i)), Masson's trichrome (B(i)), and alcian blue (C(i)) staining were performed, and images were analyzed for percentage of remaining visible nuclei (A(ii)), percentage collagen (B(ii)), and saturation per pixel (C(ii)) using custom MATLAB algorithms. Scale = 100 μ m. Magnification of 20 \times . *n*

5. Ordinary one-way ANOVAs/Tukey's tests were performed using GraphPad Prism 9.1.0. Shared letter designations (A–C(ii)) indicate groups that are not statistically significantly different ($p < 0.05$).

**Figure 4.**

IHC to evaluate for retained ECM proteins. Collagen I, collagen IV, fibronectin, laminin, chondroitin sulfate, and heparan sulfate content were evaluated (A), and mean pixel intensities (MPI) were analyzed (B) using Fiji ImageJ. Scale = 100 μ m. Magnification of 20 \times . $n = 3$. Ordinary one-way ANOVAs/Tukey's tests were performed using GraphPad Prism 9.1.0. Shared letter designations (B) indicate groups that are not statistically significantly different ($p < 0.05$).

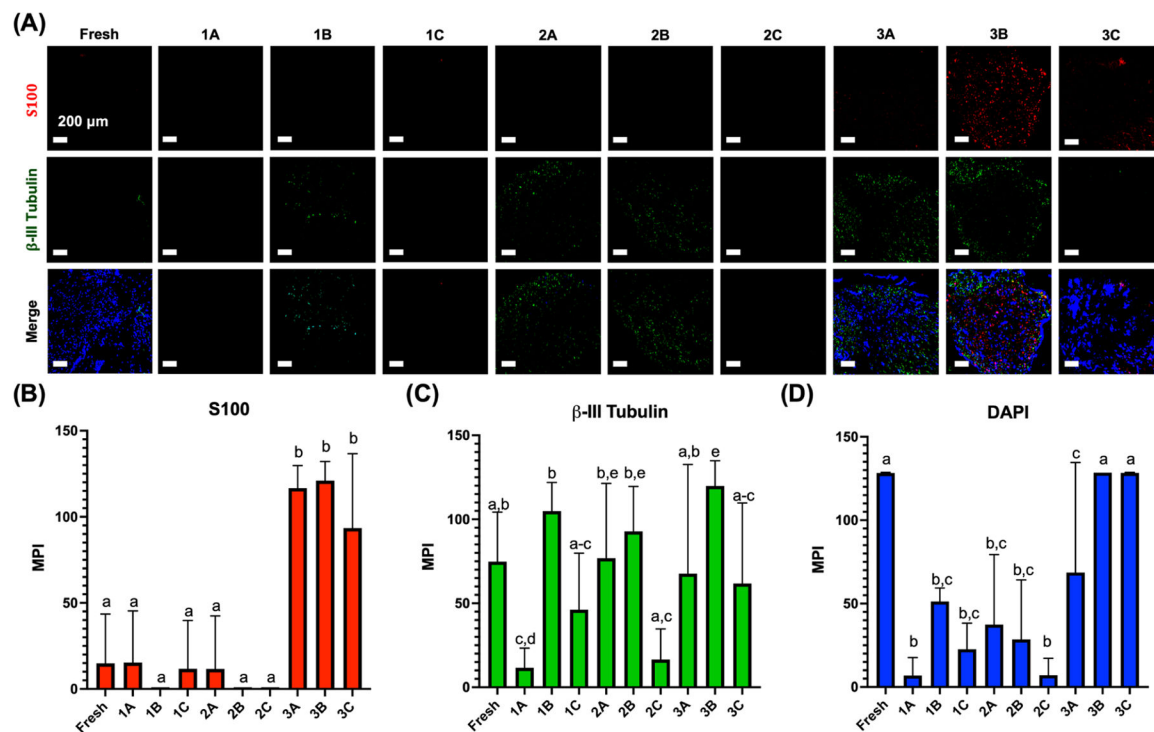


Figure 5.

IHC to evaluate for remaining cells. IHC was performed against S100, β -III tubulin, and DAPI (A) for fresh and decellularized nerves and analyzed (B–D) using Fiji ImageJ. Scale = 200 μ m. Magnification of 10 \times . $n = 6$. Ordinary one-way ANOVAs/Tukey's tests were performed using GraphPad Prism 9.1.0. Shared letter designations (B–D) indicate groups that are not statistically significantly different ($p < 0.05$).

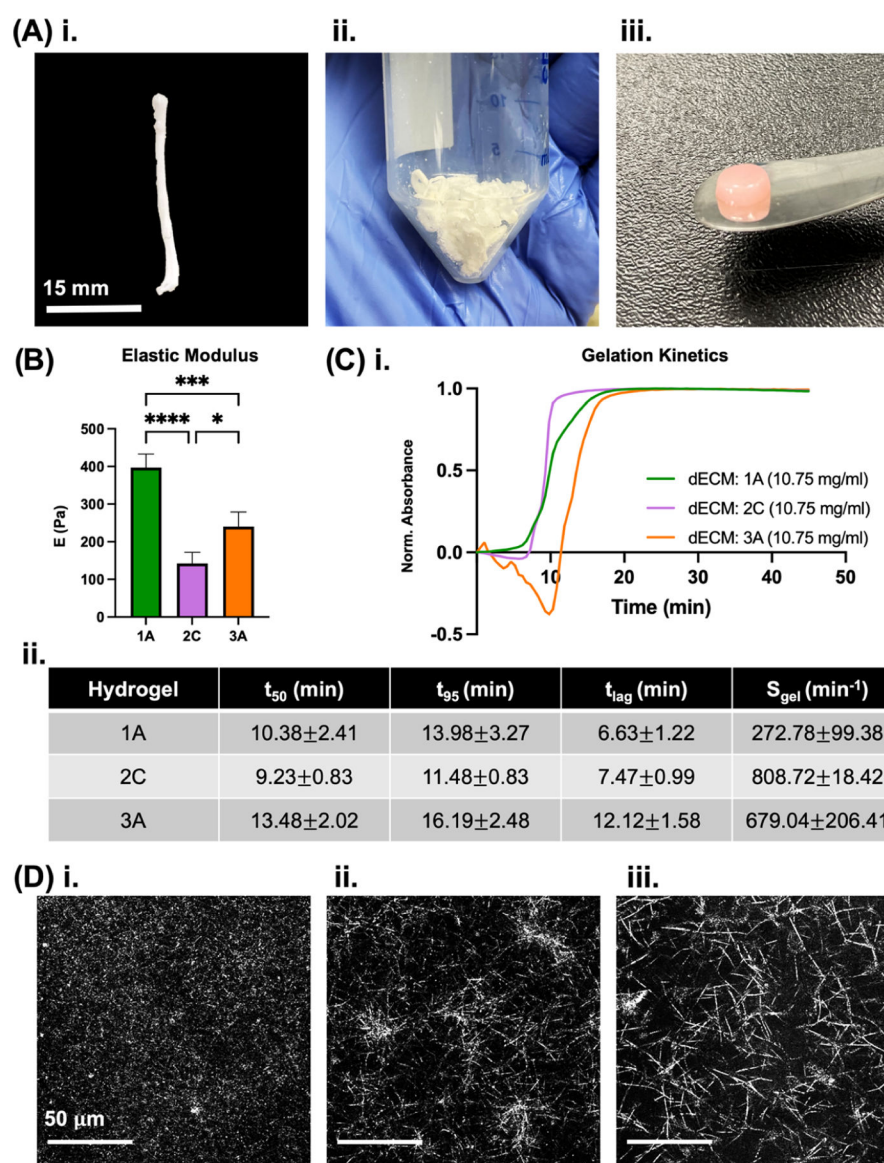
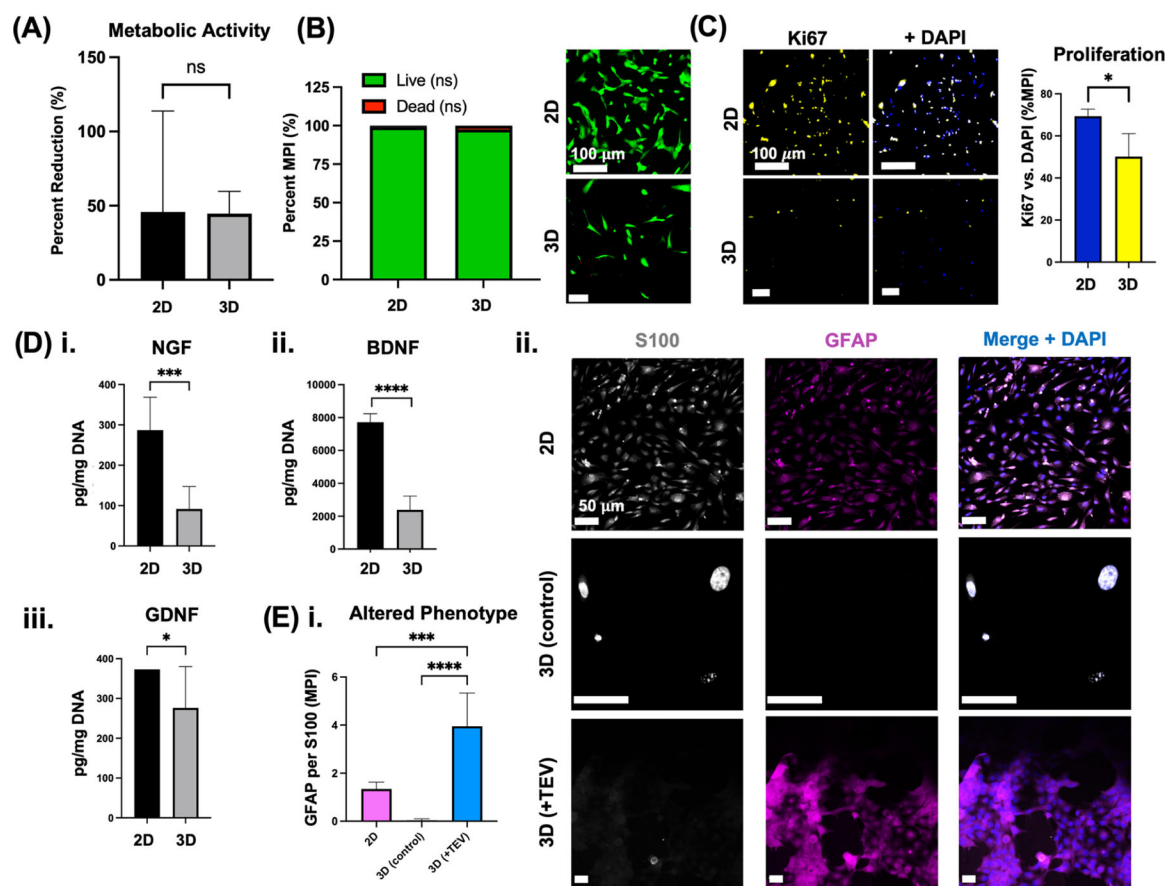


Figure 6. Hydrogel fabrication and characterization. Sprague Dawley rat sciatic nerves were isolated (A(i)), decellularized and lyophilized (A(ii)), and then digested into dECM hydrogels of the best of each decellularization method (A(iii)). Scale = 13 mm. Rheological characterization was implemented to evaluate the elastic modulus of each hydrogel (B). Gelation kinetics was performed (C(i)) and used to establish the times to 50 and 95% gelation (t_{50} and t_{95} , respectively), the lag time prior to gelation (t_{lag}), and the speed of gelation (S_{gel}); Data are presented as mean \pm standard deviation. Confocal reflectance imaging was utilized to determine collagen fibrillar network structure in the hydrogels (D). Scale = 50 μ m. $n = 3$. Ordinary one-way ANOVAs/Tukey's tests were performed using GraphPad Prism 9.1.0. * $p < 0.05$, *** $p < 0.005$, **** $p < 0.0001$.

**Figure 7.**

Schwann cell culture in 2D and 3D. Cell metabolism (A) was analyzed 3 days of culture on coverslip (2D) and in hydrogel (3D) via alamarBlue. Live/Dead fluorescent staining (B) was used to evaluate the viability of 2D- and 3D-cultured Schwann cells, and mean pixel intensities (MPI) of live versus dead cells were compared. Scale = 100 μ m. IHC was performed against Ki67 proliferation marker (C). Luminex analysis of NGF, BDNF, and GDNF was performed, and analyte concentrations were normalized by dsDNA concentration (D). Hydrogel-embedded Schwann cells were treated with pancreatic tumor-derived extracellular vesicles (TEV), and IHC was performed against S100 and GFAP markers (E). DAPI is depicted in blue. Scale = 50 μ m. $n = 3$. One-way ordinary ANOVA/Tukey's test (B), two-way ANOVA/Sidak's test (F), and unpaired t -tests (G–J) were performed using GraphPad Prism 9.0; * $p < 0.05$, *** $p < 0.005$, **** $p < 0.0001$.

Table 1.Decellularization Method and Preparation Ranking^a

Analysis	1A	1B	1C	2A	2B	2C	3A	3B	3C
dsDNA	1	2	3	9	4	7	5	8	6
Cytotox.	4	2	6	8	1	3	5	7	9
H&E	2	1	3	8	9	6	5	4	7
Trichrome	3	2	1	6	5	4	7	9	8
Alcian Blue	4	2	7	6	1	5	8	3	9
S100	4	1	3	2	1	1	6	7	5
B-III Tub.	1	8	3	6	7	2	5	9	4
DAPI	1	6	3	5	4	2	7	9	8
Collagen I	2	6	3	7	4	1	9	8	5
Collagen IV	2	7	8	3	5	1	6	9	4
Fibronectin	1	5	7	3	2	4	6	9	8
Laminin	1	6	7	2	3	4	5	9	8
CSPG	5	7	9	8	2	4	1	6	3
HSPG	5	8	7	9	4	6	1	3	2
Sum	36	63	70	82	52	50	76	100	86

^aMethod groups were ranked from 1 to 9 (1 being the best, 9 being the worst) based on successful DNA and cell removal, low cytotoxicity, and high ECM protein retention. Abbreviations: dsDNA, double-stranded DNA; H&E, hematoxylin and eosin; B-III tub., β -III tubulin; CSPG, chondroitin sulfate proteoglycan; HSPG, heparan sulfate proteoglycan.